ACI STRUCTURAL JOURNAL TECHNICAL PAPER

Title No. 113-S112

Shear Response under Reversed Cyclic Loading

by David M. Ruggiero, Evan C. Bentz, Gian Michele Calvi, and Michael P. Collins

A series of three shear panels with transverse reinforcing ratios ranging from 0.23 to 0.68% were tested to failure under reversed cyclic loading. All of the tests showed a reduction in strength of at least 20% with respect to predictions from reliable monotonic analyses. Extensive experimental results including strain distributions and cracking patterns were analyzed to explain this discrepancy, and it was determined that shear behavior under reversed cyclic conditions is not well captured by a single rotating crack model; rather, explicit consideration of both diagonal crack systems is required. This analysis has shown that the behavior can be rationally explained by considering the evolution of crack slip and crack closing hysteresis.

Keywords: crack closing; crack slip; reinforced concrete; reversed cyclic loading; shear behavior; shell element tester.

INTRODUCTION

During events such as earthquakes, buildings and other structures can be subjected to large lateral loads of alternating direction. The effects of such "reversed cyclic" loading have been studied at length in the field of seismic engineering and much effort has been devoted to determining the implications for reinforced concrete (RC) components such as walls and columns.[1] While flexural mechanisms are well understood today, questions still remain about cyclic shear behavior. In spite of the adoption of a capacity design philosophy in modern codes to preclude shear failures, damages from recent earthquakes have demonstrated that shear is still a pressing problem in seismic design.[2]

Traditionally, it is assumed that the shear capacity of an RC member is significantly reduced when the main longitudinal reinforcement has yielded (that is, within a flexural hinge), and this is reflected in design codes and analytical models.[3] However, previous work by Stevens et al.[4] has shown that a reduction in shear resistance may also occur in regions where there is no flexural hinging. Examples of failures in such regions are shown in a real-world context in Fig. 1. Experimental data on the topic is sparse, however, and the mechanisms of this behavior are still not well understood. To provide further quantification of this effect, therefore, a more comprehensive study into the reversed cyclic shear behavior of reinforced concrete is required.

Several models describing the mechanics of RC panels under reversed cyclic shear have been proposed over the last 30 years[4-12]; however, they vary in generality and applicability and there is still a lack of consensus as to the effects of cycling on shear strength and behavior. A full review of the strengths and weaknesses of these previous efforts may be found elsewhere.[13]

One reason for the lack of a general model for reversed cyclic shear behavior is the difficulty of conducting reversed cyclic pure shear tests; only a few experiments of this nature are recorded in literature[4,6,9,14-17] and they do not exhaustively consider all the different parameters that affect the response (such as reinforcing ratios and concrete strengths) Nonetheless, the general trend in the results indicates that under reversed cyclic shear loading, the strength of an element decreases and the deformations increase when compared to a comparable monotonic test. This implies that cyclic shear loading causes significant degradation of shear strength, even outside of regions of flexural yielding. In a design context, this could effect a reduction in actual factors of safety and cause elements that were designed to be ductile to be shear critical in reality.

An understanding of why existing monotonic models cannot simply be used as a backbone for cyclic predictions is a prerequisite to the formulation of a model that can accurately describe the detailed reversed cyclic shear behavior of reinforced concrete. By examining the assumptions of proven monotonic models, such as the modified compression field theory (MCFT),[18] one can determine what aspects of reversed cyclic behavior are fundamentally different from the monotonic case.

This paper presents the results of three of a series of reversed cyclic shear experiments that were conducted at the University of Toronto to gain a better understanding of reversed cyclic shear behavior in reinforced concrete. These tests were designed to add to the limited experimental literature about specimens with unequal reinforcement in the x and y directions. Detailed investigation of the experimental results, including new techniques for calculating and presenting crack slips and widths, will be used to assess how suitable existing monotonic procedures are for analyzing reversed cyclic shear loading, and to lay the groundwork for a rational, analytical model for reversed cyclic shear behavior.

RESEARCH SIGNIFICANCE

The results of three experiments in which reinforced concrete panels were subjected to reversed cyclic shear loading are presented herein. All three tests demonstrate a significant strength reduction with comparison to monotonic predictions, indicating that existing procedures for assessing

ACI Structural Journal, V. 113, No. 6, November-December 2016.

MS No. S-2015-403.R1, doi: 10.14359/51689033, was received November 28, 2015, and reviewed under Institute publication policies.

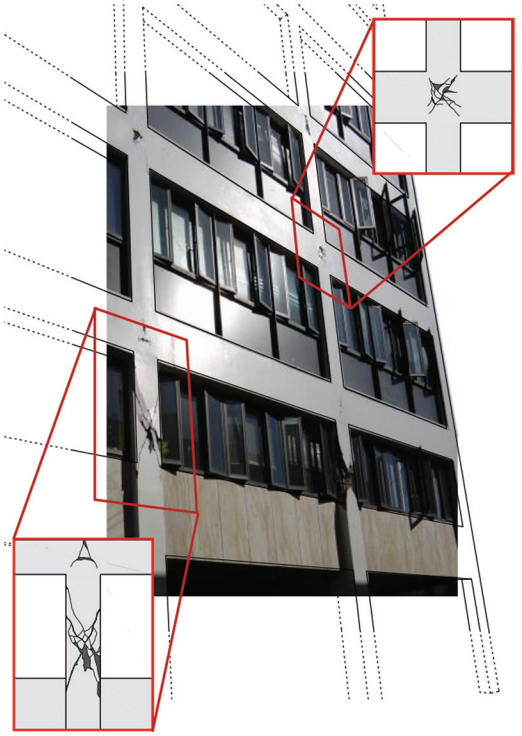

Fig. 1—Examples of reversed cyclic shear failure in real-world structure (2011 Christchurch, New Zealand, earthquake).

shear strength can be unconservative under non-monotonic loading conditions. The data from the tests is presented using novel techniques which highlight why rotating crack models may be ill-suited for detailed analysis of reversed cyclic shear behavior.

EXPERIMENTAL PROGRAM

The three specimens considered in this paper (labelled SR3, SR5, and SR7) form a subset of a larger collection of 10 tests performed using the University of Toronto's Shell Element Tester (SET); full details of the experimental program including numerical data may be found elsewhere.[13] The SET is a general testing frame used to apply uniform stress states to full-scale reinforced concrete shell elements. By applying principal stresses horizontally and vertically and choosing an appropriate orientation for the reinforcing bars, any in-plane stress state can be achieved. For the case of pure shear loading, the longitudinal (x direction) and transverse (y direction) reinforcing must be oriented at 45 degrees to the horizontal and vertical axis system (refer to Fig. 2). In reversed cyclic loading, the in-plane loads are scaled proportionally to create both positive and negative shear. A full cycle will therefore first induce tension horizontally and compression vertically, then reverse to apply compression horizontally and tension vertically.

Loading is applied around the perimeter of the specimen via 40 in-plane and 20 out-of-plane actuators. The actuators are pinned to loading yokes and react against the frame of the SET. The loading yokes are fastened via high-strength bolts to anchor blocks in the concrete, while the anchor blocks themselves are welded to the steel reinforcing cage. Thus, both tension and compression may be applied directly

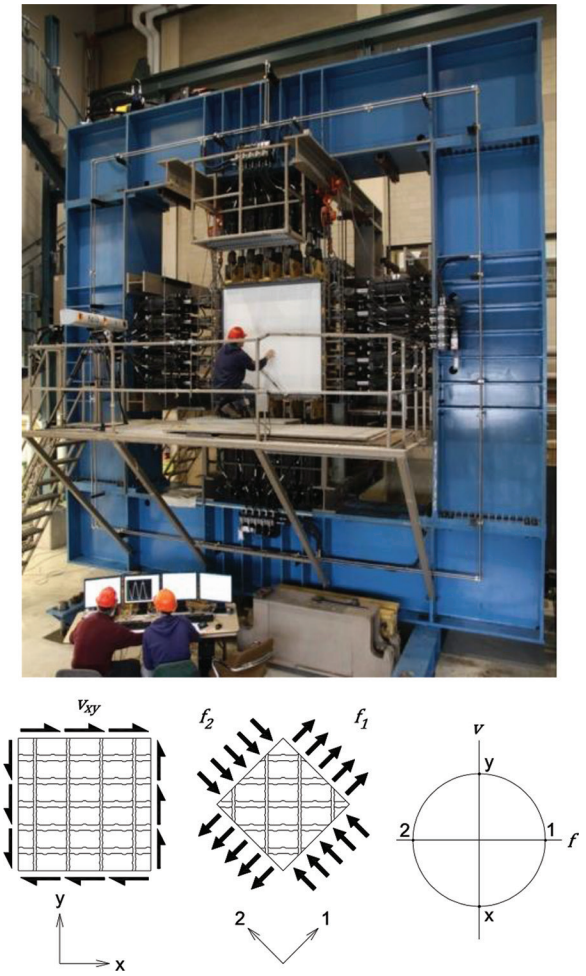

Fig. 2—North face of Shell Element Tester at University of Toronto (top); creation of state of pure shear stress by application of principal tension and compression diagonal to reinforcement axes (bottom).

to the specimen. More details about the general configuration of the SET are reported by Kirschner and Collins[19] and Khalifa.[20]

The SR test series was the first to use the SET after a major upgrade was performed in 2009, converting all 60 of the actuators to servo control. In the new configuration, each actuator can be individually commanded in either force or displacement control, using feedback provided by a string potentiometer measuring ram displacement and a load cell measuring applied force. The system is controlled by computer software that is typically used in the aerospace industry for large-scale structural testing.

Details of SR3, SR5, and SR7 are provided in Table 1. Each specimen was designed to be nominally 1626 x 1626 x 285 mm (64 x 64 x 11.2 in.), and was reinforced with two layers of deformed steel bars in each of the x- and y-directions (refer to Fig. 3).

The three specimens form a series with equal x direction reinforcement and increasing amounts of reinforcement in the y direction according to the ratios 1:2:3. SR3 was also reinforced with additional stub bars around its perimeter to aid with the transfer of tension into the concrete. Canadian 20M steel bars were used for the x-direction reinforcement,

Table 1—Summary of experimental program

Test	f_c', MPa	t, mm	$\rho_y f_{yy}$, MPa	ρ_x, %	x reinforcement, mm	f_{yx}, MPa	Age at testing, days	Loading history, No. × MPa	v_{crack}, MPa	v_{max}, MPa	v_{MCFT}, MPa	v_{max}/v_{MCFT}
				ρ_y, %	y reinforcement, mm	f_{yy}, MPa						
SR3	28.9	289	1.12	2.89	20M @ 71.8	411*	53	3 × ±1.50 5 × ±2.30 3.5 × ±2.50	+2.30 –2.20	+2.50	3.10	80.6%
				0.228	US No. 3 @ 216†	492						
SR5	49.5	292	2.22	2.86	20M @ 71.8	411*	25	3 × ±3.20 3 × ±3.50 3.5 × ±3.80	+3.10 –2.90	–3.80	5.22	72.8%
				0.451	US No. 3 @ 108	492						
SR7	32.6	293	3.32	2.85	20M @ 71.8	453*	28	3 × ±2.60 3 × ±3.50 4.5 × ±4.50	+2.50 –2.00	+4.50	5.90	76.3%
				0.675	US No. 3 @ 71.8	492						

*SR3 and SR5 used steel 20M-1, while SR7 used 20M-2.

†Additional 174 mm No. 3 stubs were added around perimeter to aid transfer of tension into concrete.

Notes: 1 mm = 0.0394 in.; 1 MPa = 0.145 ksi.

while U.S. No. 3 bars with an ultimate tensile strength of 598 MPa (86.7 ksi) were used for the y direction. Ready mixed concrete with a specified strength of 25 MPa (3.6 ksi) was used in each case. The concrete strengths on test day as determined by three 150 x 300 mm (6 x 12 in.) cylinders varied widely and are reported in Table 1.

Data acquisition for the experiments was extensive; an average of over 50 GB of storage space for numerical data, photos, and videos was required per test. Of primary importance were the continuous recordings of forces (by the actuator load cells) and displacements. A total of 28 strain gauges were installed directly on reinforcing bars to monitor strains in the x- and y-directions, as well as out-of-plane using thin bulging gauges. Six linearly varying differential transformers (LVDTs) were installed on each face of the specimen to record the average strain state, while a grid of 25 infrared light emitting diodes (LEDs) was positioned on the south face of the specimen and tracked by a three-dimensional (3-D) scanner to give continuous, position-varying strain readings (Fig. 3). Additionally, at key points during testing (load stages), the loading was paused so that crack patterns could be traced and their widths measured at several locations along their lengths.

The specimens were loaded in reversed cyclic shear using force control. The amplitude of the cycles at a given stage of testing was kept constant for three to five cycles depending on the observed damage. The specimens were first cycled three times at the stress which caused cracking, with the exception of SR3, which was also cycled before cracking to verify the behavior in the linear elastic regime. Following cracking, the shear stress amplitude was increased until significant stiffness degradation was observed and cycling of the loads continued at that level. When the degradation at a particular stress level appeared to have stabilized (that is, no significant increases in strain on subsequent cycles), the amplitude was increased and the process was repeated until failure. SR5 and SR7 exhibited sufficient ductility to be reloaded after failure in order to capture some of the post-peak behavior.

Post-processing of the data was performed with a purpose-built program used to synchronize all of the various data streams. Data reduction was conducted where necessary to reduce the dataset to a manageable size while retaining the high-resolution source files for future investigation.

EXPERIMENTAL RESULTS

The observed behavior of each of the three tests followed a similar pattern. Upon loading in the positive shear direction, one or more cracks formed suddenly in a nearly vertical orientation. When the sense of the loading was reversed, analogous cracks formed nearly horizontally under negative shear stress. It should be kept in mind that the horizontal and vertical orientation of the cracks corresponds to diagonal (±45 degrees) cracking in the x-y coordinate system. Subsequent cycles at the cracking load caused additional cracks to form, though the alignment of the new cracks skewed slightly more towards the direction of the x reinforcement, as expected according to the stiffness anisotropy of the reinforcing steel. Increasing the loading amplitude caused a densification of the pattern of crossing cracks and evidence of damage (for example, chipping, flaking, and spalling) on the surface of the specimens. Failure of each of the three specimens was sudden and brittle, accompanied by extensive spalling over a large area of the panel and significant sliding on one or more large shear cracks. Subsequently, the interior of the specimen was reduced to coarse rubble, held together loosely by the reinforcing cage, indicating that crushing of the concrete had also occurred.

Because the specimens were loaded in pure shear, the behavior is best characterized by the shear stress versus shear strain plots shown on the left side of Fig. 4. The shear stress was obtained by dividing the sum of the measured actuator forces by the cross-sectional area of the test region. The shear strain as plotted was calculated using the measured displacements of four perimeter LED targets so as to obtain an average strain over the test region; there was good agreement between these values and those recorded directly by the LVDTs.

The middle column of Fig. 4 shows the behavior in the form of "exploded hysteresis" plots. Each complete cycle of the response is plotted independently, offset on the strain axis for clarity. From these plots, the characteristic shape of the behavior at each stage of cycling can be discerned. Cycles conducted prior to cracking (such as for SR3) are

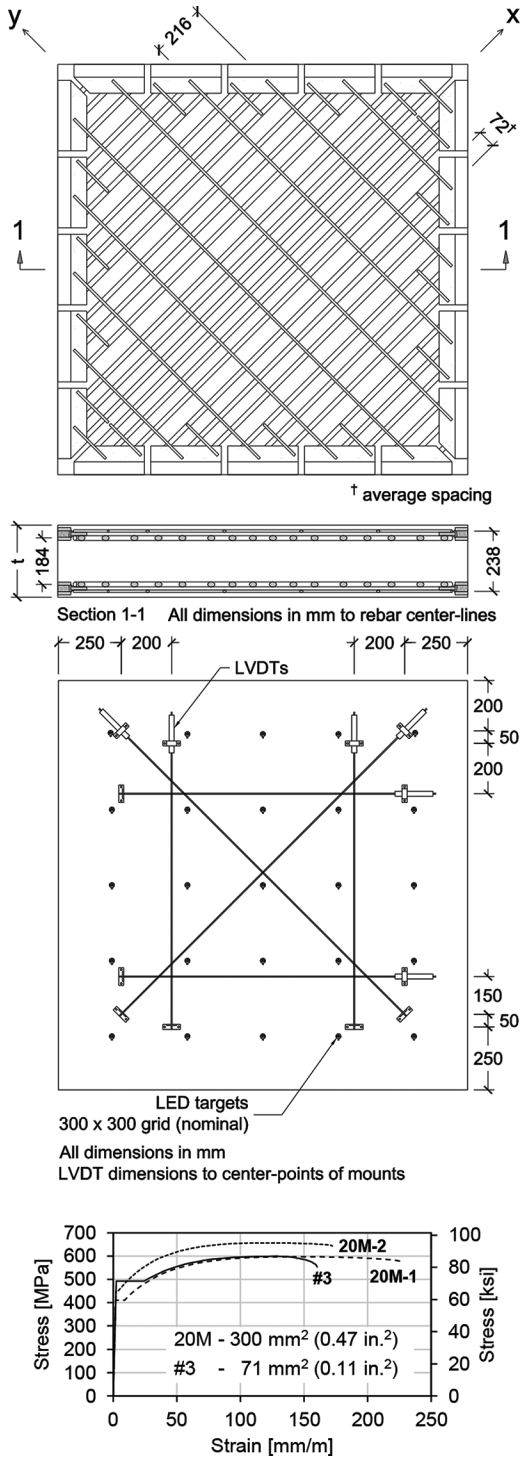

Fig. 3—Construction details (top) and surface instrumentation (middle) for SR3; reinforcing steel stress-strain curves (bottom). (Note: 1 mm = 0.0394 in.)

virtually linear elastic, with no apparent degradation due to reversal of the load. Upon increasing the shear stress amplitude, cracking is observed first in the positive direction (vertical cracks), and then in the negative direction (horizontal cracks). No drop in force readings occurs during cracking (as evidenced by the horizontal line segments on the plots), indicating that the controller was effective in maintaining load control. Upon reloading to the cracking stress, the hysteresis loops take on a stretched diamond form, with stress and strain offsets near the origin tapering to sharp points at the peaks.

The nature of the reversed cyclic behavior changes at higher load levels. Experimentally, this change corresponds to the first instances of yield in the y-direction reinforcement as confirmed by the strain gauge readings. Instead of tapering to a point, at high loads, the cycles become elongated and appear to plateau. Upon unloading, a high tangent stiffness is maintained until the shear changes sign, at which point the stiffness drops significantly. Stiffness is then gradually regained as loading progresses in the opposite sense until the corresponding negative plateau is reached.

Real-time monitoring as well as post-processing of the strain gauge readings confirmed that while the y-direction reinforcement yielded extensively, the larger bars in the x-direction did not yield prior to failure. Therefore, these tests are analogous to structural elements outside of flexural hinging zones; for example, short coupling beams or beam-column joints.[21]

The failure shear strengths of the three specimens are compared to the monotonic shear strengths predicted by the MCFT in Fig. 5. The results of six comparable monotonic experiments,[13,22] as well as one additional reversed cyclic experiment,[4] are also shown for reference. In all cases, the specimens tested under reversed cyclic loading failed at loads significantly lower than the MCFT predictions. This is outside of the typical range of statistical fluctuation for the MCFT,[22] and therefore suggests a systematic effect. Furthermore, the reduction was more pronounced for the more heavily reinforced panels; SR3 showed a 19% reduction of load-carrying capacity relative to the prediction, while SR5 and SR7 showed 27% and 24% reductions in peak stress, respectively. To explain these strength reductions, as well as the inability of the monotonic model to reproduce the envelope of the reversed cyclic hysteresis loops, it is informative to investigate in more detail some of the assumptions of the MCFT and to test (using the reversed cyclic data) how they fare in the case of non-monotonic loading.

PRINCIPAL STRESSES AND STRAINS

The MCFT is a rotating crack model that treats cracked concrete as a distinct, orthotropic material. Its formulation is based on the laws of compatibility, equilibrium, and three constitutive assumptions, namely:

1. The concrete principal tensile stress depends on the principal tensile strain as per a "tension stiffening" relationship;
2. The concrete principal compressive stress depends on the principal compressive and tensile strains as per a "compression softening" relationship; and
3. The angle of principal stress in the concrete is coincident with the overall angle of principal strain.

These assumptions have previously been shown to work very well for the monotonic case,[22] but their applicability to reversed cyclic loading scenarios is more questionable.

To validate or refute the MCFT assumptions, it is necessary to back-calculate the stress state in the concrete during the experiments. This can be achieved using the procedure of Vecchio and Collins,[18] in which the stress state of the steel is subtracted from the total applied stresses to give the stress

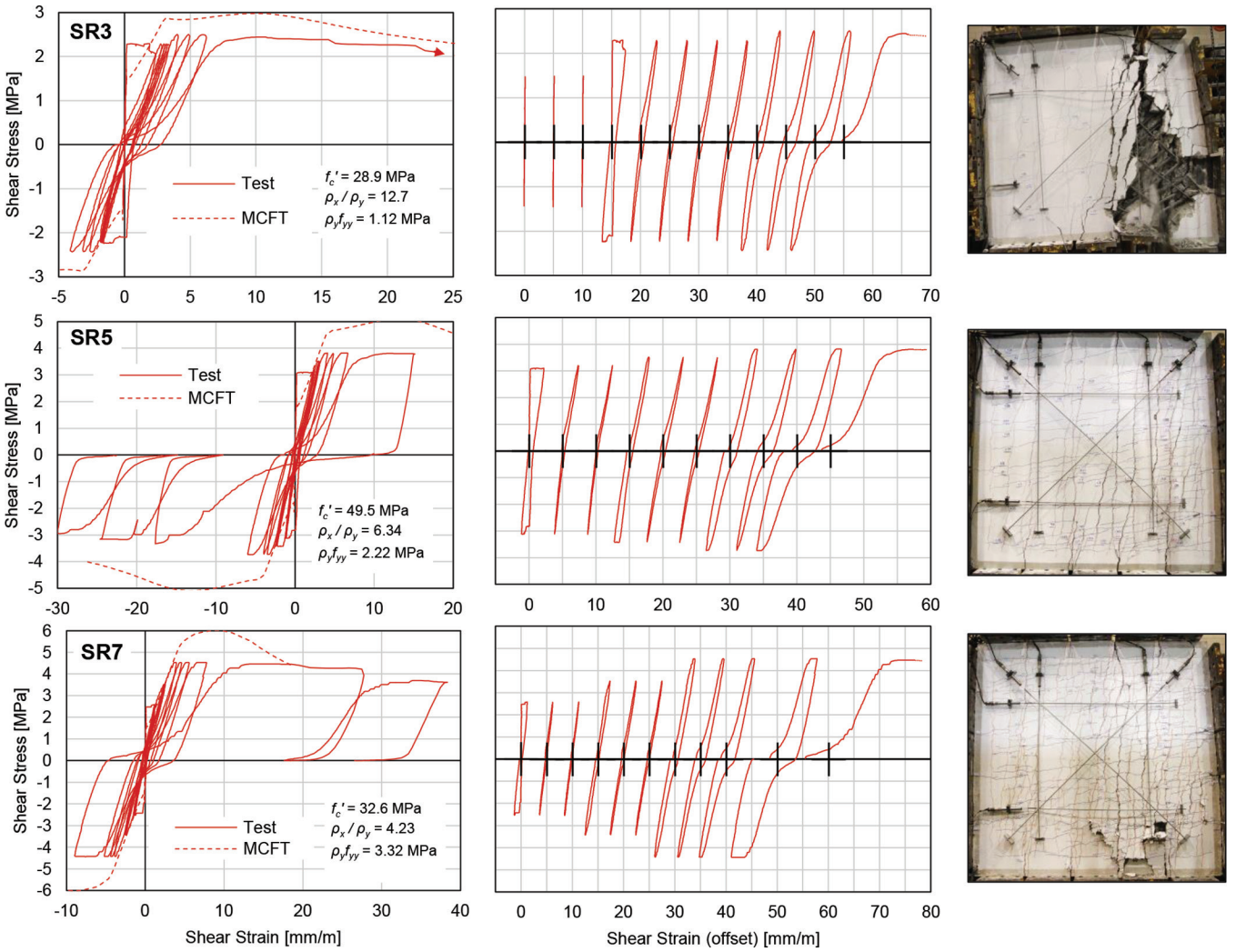

Fig. 4—Shear stress versus shear strain, plotted with MCFT prediction (left) and as exploded hysteresis diagrams (middle); photo at failure (right). (Note: 1 mm = 0.0394 in.; 1 MPa = 0.145 ksi.)

tensor of the concrete alone. The stresses in the reinforcing steel are calculated based on the strains in the reinforcing bars as calculated from the LVDT readings and the measured bare bar stress-strain response of the reinforcement. In tensor notation

$$\{f_c\} = \{f\} - \{f_s\} \tag{1}$$

In the x-y coordinate system

$$\begin{Bmatrix} f_{cx} \\ f_{cy} \\ v_{cxy} \end{Bmatrix} = \begin{Bmatrix} f_x \\ f_y \\ v_{xy} \end{Bmatrix} - \begin{Bmatrix} f_{sx} \\ f_{sy} \\ v_{sxy} \end{Bmatrix} \tag{2}$$

where

$$\begin{Bmatrix} f_{sx} \\ f_{sy} \\ v_{sxy} \end{Bmatrix} = \begin{Bmatrix} \rho_x f_{sx,bar} \\ \rho_y f_{sy,bar} \\ 0 \end{Bmatrix} \tag{3}$$

Plots of the tensile and compressive behavior for SR7 are shown in Fig. 6 (top), along with the corresponding MCFT predictions. Principal strains have been calculated from LVDT readings. The plots for SR3 and SR5 are omitted herein for brevity; they demonstrate similar trends as SR7.

The experimental plots show significant deviations from the monotonic model response and no consistent pattern emerges from the experimental data when visualized in principal strain directions. In the case of the tensile behavior, though the MCFT tension stiffening relationship provides a good envelope to the data, unloading and reloading radiate back towards an intercept of approximately 1 MPa (0.145 ksi) of compression on the stress axis and show some irregular stiffness reversals under compressive stress. Data at high strain levels is more erratic, likely indicating the limits of the bare bar assumption for the steel stress component.

The predictions for compressive stress provide a poorer envelope of the actual experimental data. The peak concrete stress obtained in the experiment is only a fraction of that predicted by the MCFT compression softening relationship. Furthermore, during many cycles, the behavior ventures into the tensile strain quadrant (plotted here on the left side of the axis) while stresses are still compressive. This suggests that pre-existing cracks are not closing completely, such that the strain remains tensile even while the stress is compressive.

Some insight into these discrepancies can be obtained by scrutinizing the third assumption of the MCFT listed above; namely, that the angle of principal stress in the cracked concrete coincides with the angle of principal strain. The changing values of the angles of principal stress in the concrete and the angles of principal strain as loading progresses are shown in Fig. 6 (bottom).

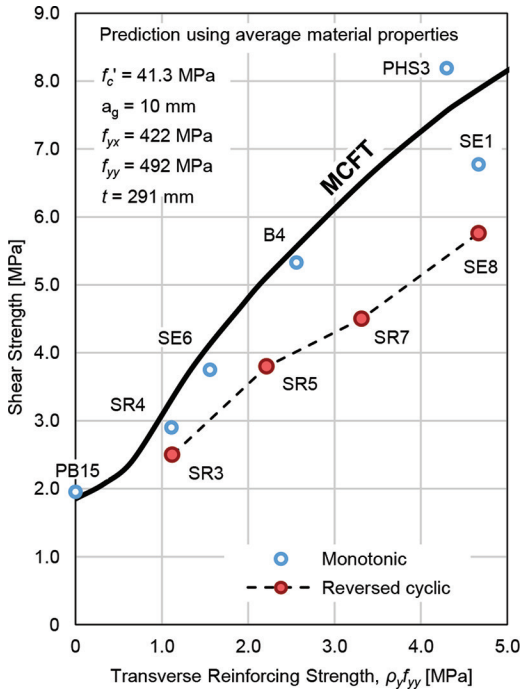

Fig. 5—Comparison of observed strengths and trend predicted by MCFT for varying transverse reinforcement. (Note: 1 mm = 0.0394 in.; 1 MPa = 0.145 ksi.)

Because the y-axes of these plots represents angles, the top and bottom lines of the graphs (±90 degrees) correspond to the same orientation and some of the data does "wrap around." It should be noted that the values for principal stress angles are very sensitive to the assumptions of strain used in the calculation, and the apparent "backward" rotation that sometimes occurs as the shear direction changes may be an artefact of this.

It is apparent from Fig. 6 (bottom) that the assumption of equal stress and strain angles in the concrete is questionable for the case of reversed cyclic loading. The divergence between the angles of principal stress and strain is most apparent at the peaks of cycles, and this deviation grows larger as the experiments progress, reaching an ultimate angle difference of at least 20 degrees in each direction. This is double the maximum observed by Vecchio and Collins[18] for monotonically loaded panels. More importantly, the strain angle lags significantly behind the stress angle in the transition regions between positive and negative shear stress. This lag accentuates the angle divergence at these points; for small stress values, the difference in angles can be larger than 45 degrees.

The divergence between the angles of principal stress and strain in the concrete explains some of the discrepancies in the tensile and compressive behavior. Because the angles of stress and strain are not always aligned, the plots of principal stress versus principal strain obscure a hidden variable; the quantities plotted on the vertical and horizontal axes do not refer to the same coordinate system, and

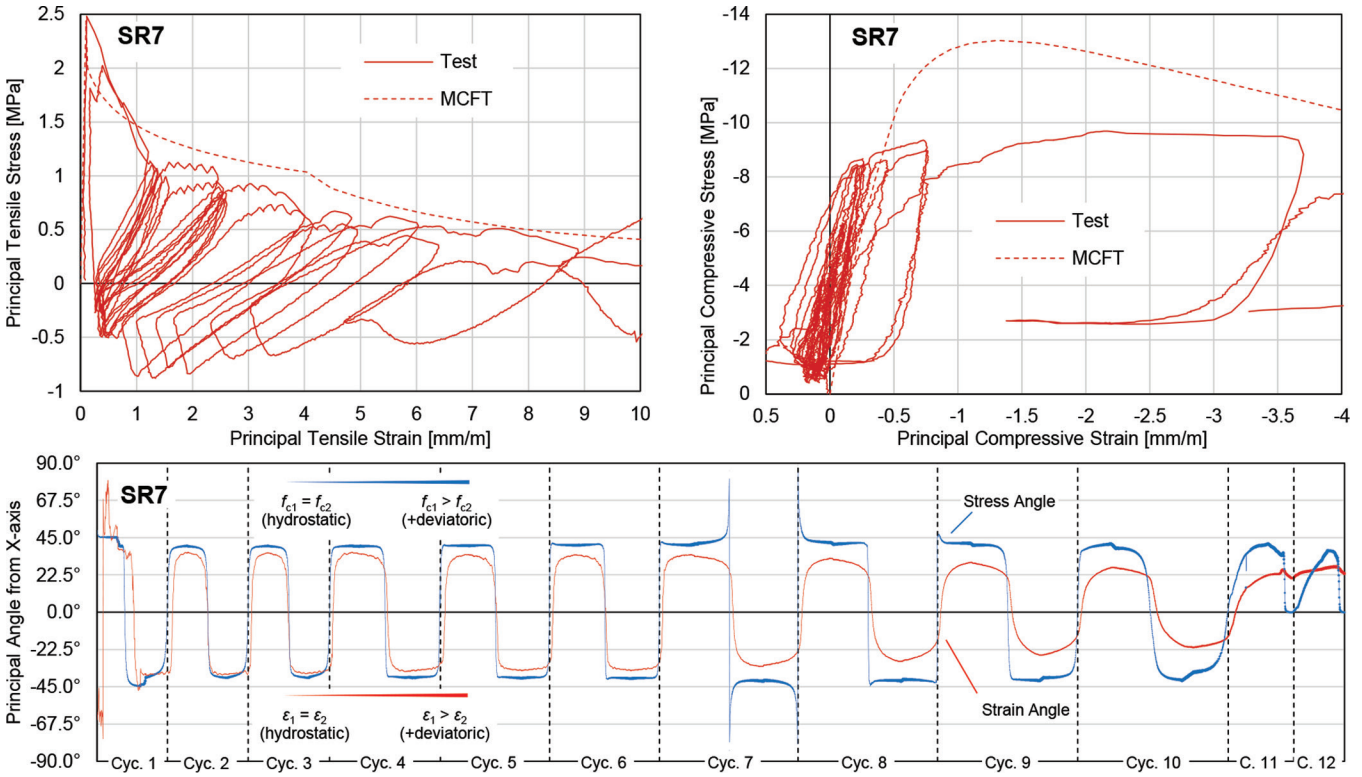

Fig. 6—Principal stresses versus principal strains calculated from LVDTs (top) and evolution of angles of principal stress and strain (bottom) for SR7. (Note: 1 mm = 0.0394 in.; 1 MPa = 0.145 ksi.)

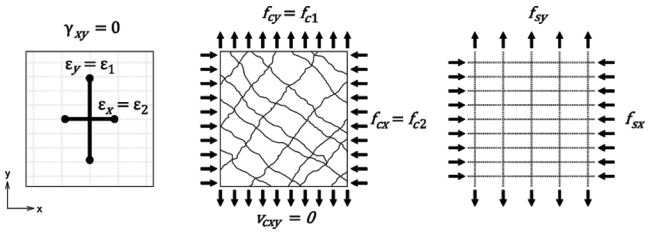

Fig. 7—Demonstration of requirement of zero shear stress for zero shear strain if equal angle assumption is upheld.

therefore it is difficult to develop constitutive relationships between them. Certain characteristics of these plots, such as apparent regions of negative stiffness near the origin, may be explained by considering that the principal stresses and strains are measured in different directions at that point in the behavior.

It can be shown that the lag between the angle of principal stress and strain is directly responsible for the diamond-shaped hysteresis (that is, the stress and strain offsets) of the reversed cyclically tested specimens. Conversely, if the stress and strain angles are constrained to be coincident, then the shear behavior is constrained to pass through the shear stress-shear strain origin. This was first noted by Stevens et al.[4] and is illustrated in Fig. 7. The leftmost panel shows a hypothetical strain state with zero shear strain in the x-y coordinate system; the principal strains are therefore vertical and horizontal. Assuming (as the MCFT does) that the angle of principal stress in the concrete is the same as the angle of principal strain, then the principal concrete stresses will also be in the x- and y-directions. The total stress state (sum of concrete and steel contributions) will therefore also align with the x- and y-axes; the shear stress is necessarily zero.

As a result of this forced behavior, rotating crack models like the MCFT are fundamentally incapable of reproducing the type of hysteresis observed in reversed cyclic shear tests; they will always pass through the origin. The behavior near the origin influences energy dissipation characteristics of the panel and the residual strains that remain once the load is removed, which are important aspects of seismic design. Furthermore, damage accrued during these cycles may contribute to the weakening of the system, reducing its ultimate strength.

The discrepancy of behavior near the origin is symptomatic of a more systematic error; namely, using a rotating crack framework to analyze a situation with multiple distinct systems of cracks. Reversed cyclic shear loading is characterized by the opening of two distinct sets of cracks, whereas a rotating crack model such as the MCFT allows only for the existence of a single theoretical crack that is always oriented parallel to the principal compressive stresses. The result is that, during the transition between positive and negative shear, rotating crack models predict a crack orientation that is inconsistent with observations, as illustrated in Fig. 8. This in turn leads to calculation of erroneous stress states and can result in incorrect predictions of the behavior.

Considering that rotating crack models are not necessarily well-suited for reversed cyclic shear, it is worth re-evaluating the experimentally measured strains and stresses using a

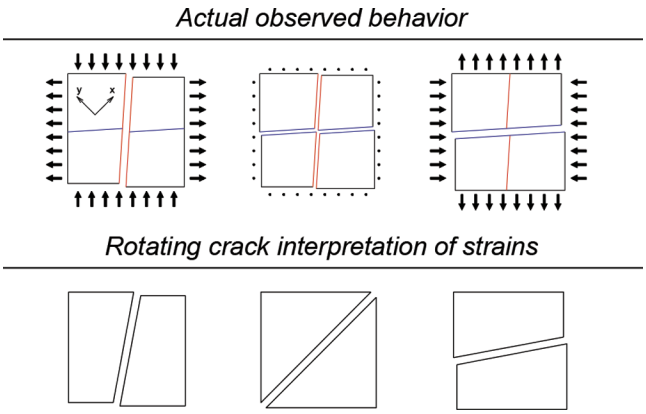

Fig. 8—Crack orientation observed in experiments and corresponding rotating crack interpretation of strain state.

fixed coordinate system aligned with the orientation of the cracks. The compatibility conditions at a crack (such as orientation, slip, and width) and crack interface stresses will be investigated in the following section.

CRACK MECHANICS

During the experiments here considered, crack patterns were traced at discrete load stages for each specimen. Afterwards, crack locations and widths for some of the tests were digitized using a custom computer program. Having the crack segment data stored internally in the program, it was therefore possible to extract statistics about the distribution of crack orientations.

Figure 9 shows a histogram for the crack angles of the south face of SR3 during the final load stage ($v_{xy} = -2.50$ MPa [–0.363 ksi], $\gamma_{xy} = -2.39 \times 10^{-3}$ mm/m), with one peak representing cracks that appeared during positive shear and the other representing cracks from negative shear. This histogram is perhaps better visualized as a "crack rose," which emphasizes the directional nature of the data. For the rose diagram, the data has been duplicated to account for the fact that angles opposite each other are equivalent.

It can be seen that the overall distribution of cracks is bimodal, with distinct peaks for the two systems of cracks. These cracks are oriented approximately horizontally (0 degrees) and vertically (90 degrees), although there is a slight average inclination towards +45 degrees from the horizontal (that is, the x-direction). This crack "rotation" is due to the unequal reinforcement ratios in the x and y directions, and it may be quantified by employing circular statistics to analyze the data.[23] Prior to failure, the circular mean angle for the "horizontal" cracks was actually 9.9 degrees, while that for the "vertical" cracks was 79.6 degrees. Therefore on average, each system of cracks formed at an angle of approximately 10 degrees from the directions of applied principal stresses.

The width of the histograms indicates that though the cracks favor a certain orientation, there is also some dispersion in the crack angle. However, quantification of this variability depends on the resolution of the crack trace and is therefore not an objective measurement; for this test, a characteristic segment length of 20 mm (0.79 in.) was used.

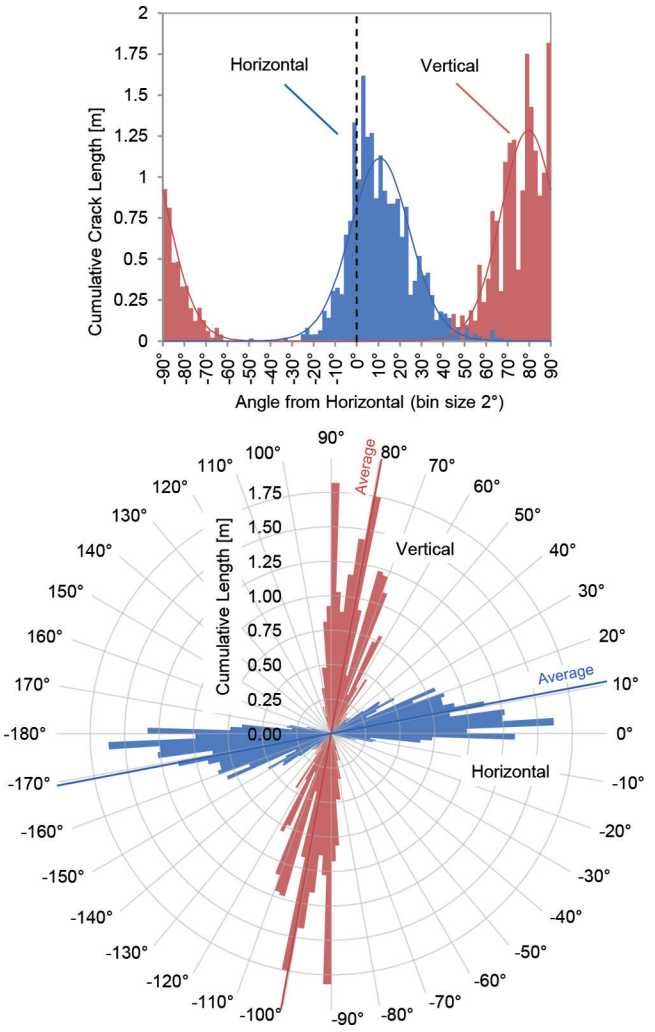

Fig. 9—Distribution of crack angles on south face of SR3, plotted as histogram (top) and as rose diagram (bottom). (Note: 1 m = 3.28 ft; 1 MPa = 0.145 ksi.)

Due to the distributed nature of the cracks in both directions, it was not feasible to measure the slips and widths of each crack in real-time during the experiments. However, making some reasonable assumptions, it is possible to infer the average slip and width from the average strain data. For cracks oriented at 0 and 90 degrees, and assuming that the deformation of the solid concrete between the cracks is negligible compared to the displacements at the cracks, the overall strain state may be expressed as follows

$$\varepsilon_h = \frac{w_v}{s_v} = \varepsilon_{cr,h} \tag{4}$$

$$\varepsilon_v = \frac{w_h}{s_h} = \varepsilon_{cr,v} \tag{5}$$

$$\gamma_{hv} = \frac{\delta_v}{s_v} + \frac{\delta_h}{s_h} = \gamma_{cr,h} + \gamma_{cr,v} \tag{6}$$

where w represents the crack width; δ represents the crack slip; s represents the crack spacing; and the subscripts h and v indicate the horizontal and vertical cracks, respectively.

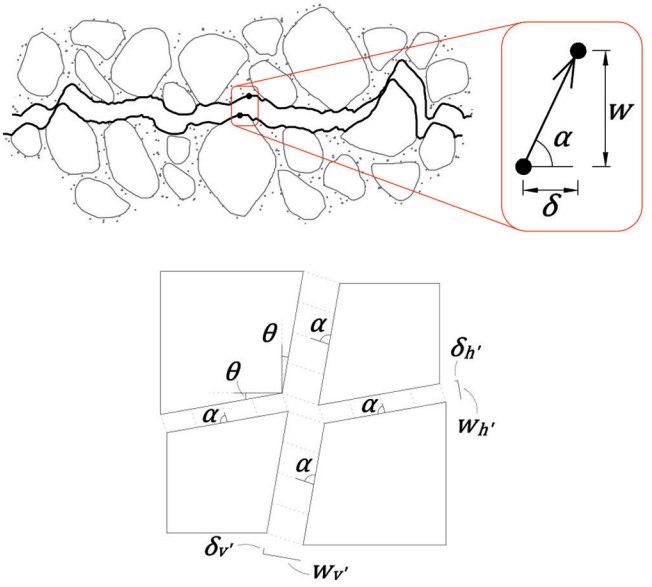

Fig. 10—Geometric definition of crack opening direction α and crack skew θ for two symmetric systems of cracks.

Because there are two independent systems of cracks, there are a total of four unknown quantities (slip and width for each system). There are, however, only three available average strain measurements from the experimental data (shear strain and two axial strains). Therefore, another constraint must be introduced to solve the equations. Given symmetric loading (that is, reversed cyclic shear), it is reasonable to assume that the level of damage of each system of cracks is the same, and that the crack spacing is the same in both directions. Previous work by Calvi[24] has shown that the amount of damage on the crack interface may be characterized by the "tooth angle" α, calculated as the arctangent of the width-slip ratio. This is represented in Fig. 10 as the angle of opening of the crack. Constraining the angles of opening to be always equal (though not constant in time) allows the following simplification

$$\tan\alpha = \frac{w_h}{\delta_h} = \frac{w_v}{\delta_v} \tag{7}$$

$$\gamma_{cr,h} = \gamma_{cr,v} \cdot \frac{\varepsilon_{cr,h}}{\varepsilon_{cr,v}} \tag{8}$$

$$\gamma_{hv} = \gamma_{cr,v} \cdot \left(1 + \frac{\varepsilon_{cr,h}}{\varepsilon_{cr,v}}\right) \tag{9}$$

$$\therefore \gamma_{cr,v} = \gamma_{hv} \cdot \left(\frac{\varepsilon_v}{\varepsilon_h + \varepsilon_v}\right) \tag{10}$$

Similarly

$$\gamma_{cr,h} = \gamma_{hv} \cdot \left(\frac{\varepsilon_h}{\varepsilon_h + \varepsilon_v}\right) \tag{11}$$

These expressions allow the slip and width of each system of cracks to be calculated as a function only of the global strain tensor (ε_h, ε_v, γ_{hv}) and the crack spacing. Crack spacing may be estimated using the formulation given by Collins and Mitchell.[25] The angle of crack opening can also be found according to

$$\tan\alpha = \frac{\varepsilon_h + \varepsilon_v}{\gamma_{hv}} \tag{12}$$

The preceding derivation assumed the cracks to be oriented at 0 and 90 degrees. The formulation taking into account the skew of the cracks from the orthogonal axes (as illustrated in Fig. 10) is more complicated but remains closed-form; its derivation may be found in full elsewhere.[13] The slip and width may be determined directly by multiplying the crack spacings by the strains, calculated as follows:

$$\varepsilon_{cr,v'} = \frac{\varepsilon_h + \varepsilon_v}{2} + \frac{\varepsilon_h - \varepsilon_v}{2} \cdot \frac{\cos 2\theta}{\sin 2\theta \cdot \dfrac{\gamma_{hv}}{\varepsilon_h + \varepsilon_v} - 1} \tag{13}$$

$$\varepsilon_{cr,h'} = \frac{\varepsilon_h + \varepsilon_v}{2} - \frac{\varepsilon_h - \varepsilon_v}{2} \cdot \frac{\cos 2\theta}{\sin 2\theta \cdot \dfrac{\gamma_{hv}}{\varepsilon_h + \varepsilon_v} - 1} \tag{14}$$

$$\cot\alpha = \frac{1}{\cos 2\theta} \cdot \frac{\gamma_{hv}}{\varepsilon_h + \varepsilon_v} - \tan 2\theta \tag{15}$$

$$\cot\alpha = \frac{\gamma_{cr,v'}}{\varepsilon_{cr,v'}} = \frac{\gamma_{cr,h'}}{\varepsilon_{cr,h'}} \tag{16}$$

Plotting the derived slips and widths for each test (Fig. 11), some trends are apparent in the data. First, the width-slip trajectories show that irreversible damage is occurring on the crack interface as the load is cycled; each loop of movement travels into a new region of the graph, and the previous regions are never traversed again on subsequent cycles. Secondly, the slip component grows consistently larger with respect to the width as the cycling progresses. For small stresses, the slip is practically zero, while towards the end of each experiment, the magnitude of the slip approaches that of the crack width.

Expressed differently, one can state that the tooth angle decreases monotonically from an initial angle of approximately 90 degrees to a final angle of approximately 55 degrees over the course of the loading (Fig. 12). The angle for each test approaches but does not cross the theoretical limit angle corresponding to crack opening purely in the y direction. Once the tooth angle degrades to this point, it is impossible to sustain any additional stress across the crack because further crack opening only serves to strain the already yielded y-reinforcement.

The scallops in the plot of crack opening angle α are due to the different paths traversed during crack opening and crack closing. The slip component is larger relative to the width during crack closing (that is, decreasing crack width) than during crack opening. This could be due to the higher compressive stresses present across the crack during closing,

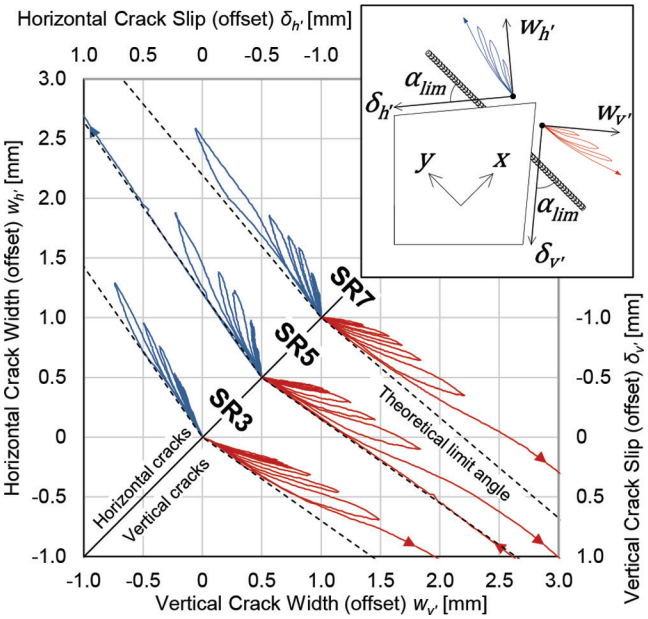

Fig. 11—Crack width versus crack slip showing theoretical limit angle. (Note: 1 mm = 0.0394 in.)

which may tend to "erode" away some of the previously intact material of the crack teeth.

The previously mentioned considerations show that, by explicitly considering the average slips and widths of each crack system, a consistent and general compatibility law can be formulated for concrete cracked in two directions. To fully describe the behavior observed in the experiments, however, it is also necessary to consider the constitutive laws that relate the strain state to the stress state. In particular, having calculated the displacements across the cracks, one may investigate how these crack displacements respond to changing stresses in the concrete across the cracks.

The procedure used previously calculated the total concrete stress tensor for each time step of each of the experiments. To calculate the stress along a particular plane (in this case, the planes of cracking), it is therefore only necessary to apply a rotation transformation. Plotting crack width against the component of stress in the concrete normal to the crack results in the graphs in Fig. 13.

When projected onto the crack directions, patterns emerge from the stress and strain data that were not apparent in principal directions. Figure 13 shows that the data is largely contained to one quadrant (tensile strain and compressive stress). Excursions into the tensile stress regime represent the residual post-cracking tensile strength of the concrete (tension softening) and the average tensile stress between the cracks (tension stiffening), and show degrading stiffness under cyclic loading consistent with prior findings.[26,27] The perpendicular behavior of the crack interfaces is similar to a nonlinear "gap element"; it is very stiff in compression and flexible in tension, offering almost no resistance to crack opening. There is a transition curve between the two branches of the response, and a hysteretic component to the behavior is evident in later cycles.

In all three of the experiments, there is a more pronounced "ratcheting" effect for the vertical cracks; the cracks do not

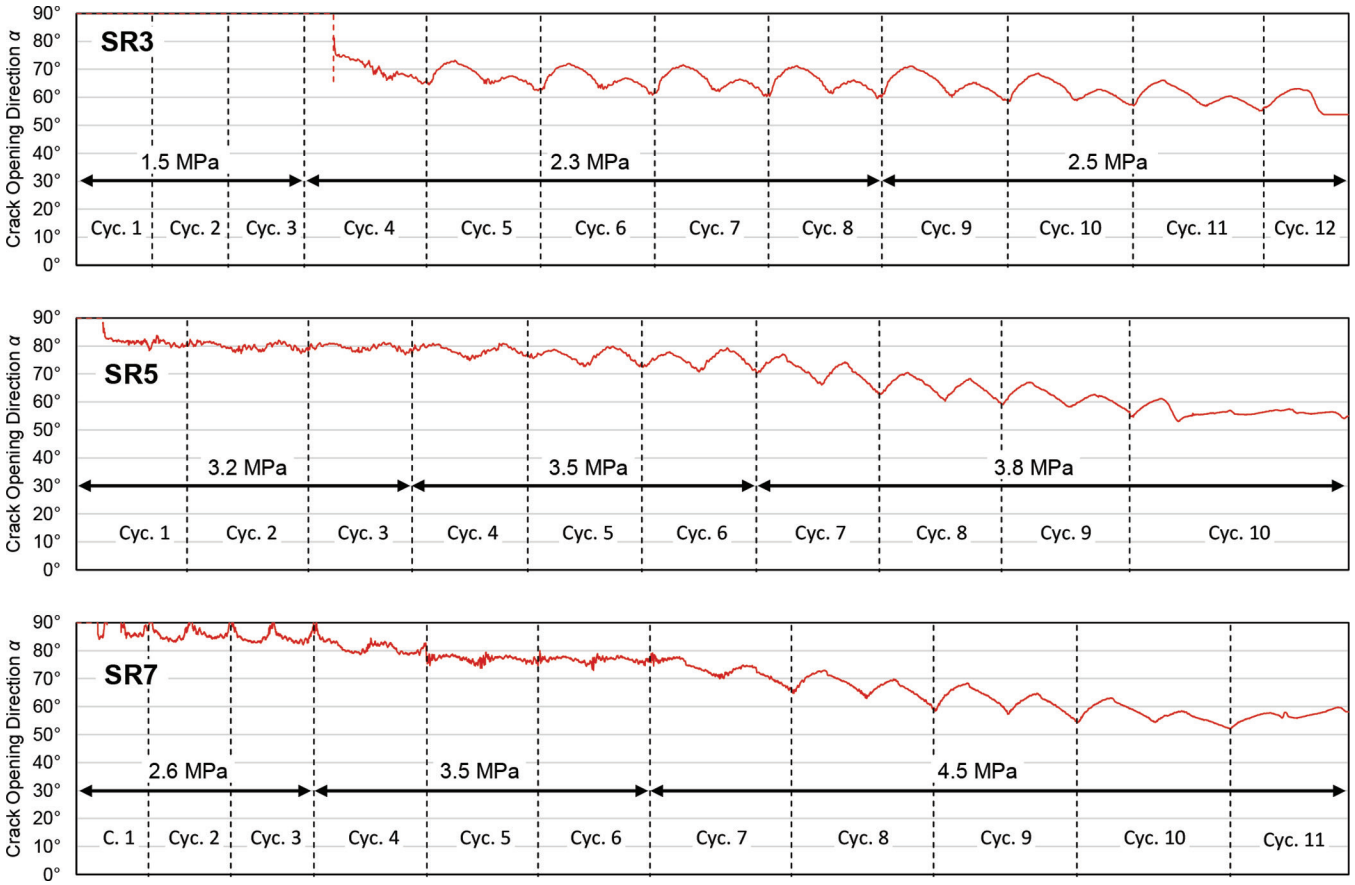

Fig. 12—Evolution of crack opening direction. (Note: 1 MPa = 0.145 ksi.)

close completely on later cycles and an increasing width offset develops. The fact that this occurs only in the vertical crack data may be an artefact of how the tests were conducted, with vertical cracks formed first. It could also conceivably be due to the orientation of the specimen, with debris falling downwards through the vertical cracks and blocking their subsequent closure. Ideally, further experiments conducted in different orientations could test this hypothesis.

In summary, while the behavior of reinforced concrete in reversed cyclic shear is complex and can appear inconsistent when viewed through the lens of a "rotating-crack" framework, it may be explained more simply by considering the cracks to be planes of discontinuity with their own constitutive behaviors. The diamond shape of the overall hysteretic loops is due to the gap-like crack-closing behavior, while the degradation of the strength and stiffness is correlated with the gradual change in the average crack tooth angle α. Accounting for both of these effects could lead to much-improved modeling of structures under reversed cyclic shear loading.

CONCLUSIONS

Through a series of full-scale laboratory experiments, it has been demonstrated that reversed cyclic shear loading of structures causes strength degradation with respect to their expected monotonic capacity. The formation of two quasi-orthogonal systems of cracks significantly diminishes the capacity of a structure to carry shear. This is of considerable consequence for seismic design because it has previously been assumed that no degradation of shear strength will be observed provided that the longitudinal reinforcement does not yield. Future design provisions should therefore recognize the significant strength degradation that can occur under reversed cyclic shear loading even outside of plastic hinge regions.

Analysis of the experimental data has shed light on why existing rotating crack models are unable to capture the hysteretic behavior observed in reversed cyclic shear tests. Such models are inherently less able to capture the interaction between two independent systems of cracks since they only allow for a single plane of cracking which rotates to sweep out all intermediate angles as the direction of loading changes.

While the reversed cyclic behavior of RC is not well-described in terms of principal directions, it has been shown that considering the material behavior in a fixed coordinate system oriented along the crack directions provides a simple explanation for the complex experimental observations for the case of reversed cyclic loading. Principal stress and strain analysis remains essential for monotonic and singly cracked RC; however, the effects of two interacting crack planes cannot be adequately represented by a single rotating crack.

The observed stress-strain behavior at the crack interfaces may subsequently be used to create an analytical model for reversed cyclic shear loading, and ultimately extended to general non-monotonic situations. In addition to informing practical recommendations regarding the design of shear

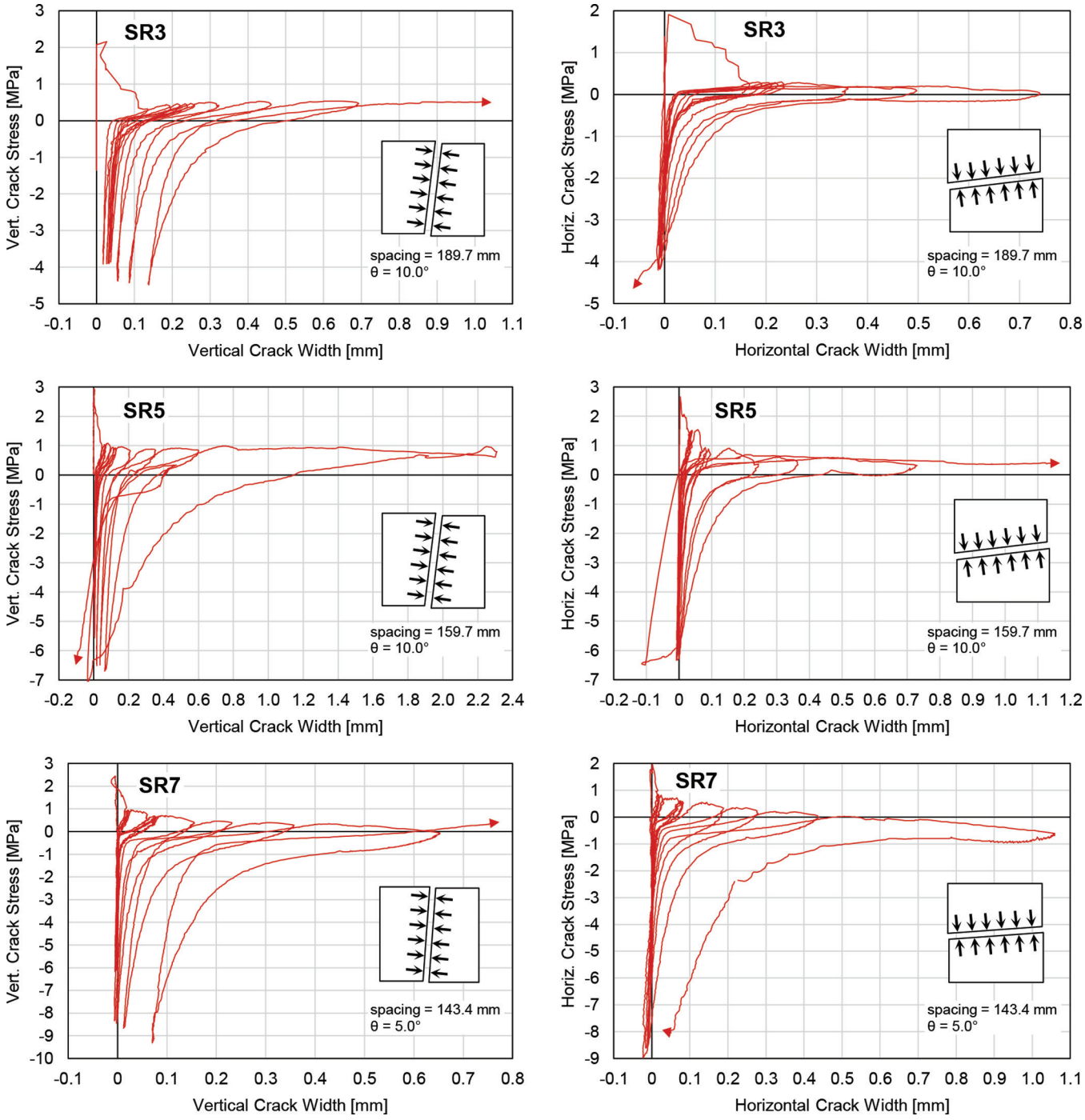

Fig. 13—Crack closing behavior, expressed as stress perpendicular to the crack versus crack width for SR3, SR5, and SR7. (Note: 1 mm = 0.0394 in.; 1 MPa = 0.145 ksi.)

panels, therefore, this research may be used form the basis for a new, rational model of reversed cyclic shear behavior in reinforced concrete.

AUTHOR BIOS

ACI member **David M. Ruggiero** *is a Researcher at the Institute for Advanced Study of Pavia (IUSS) in Pavia, Italy. He received his BASc from the University of Toronto, Toronto, ON, Canada, in 2009, and his PhD from the University of Toronto under a joint placement arrangement with IUSS in 2015. His research interests include numerical modeling of shear in reinforced concrete and seismic analysis and design of structures.*

Evan C. Bentz, *FACI, is an Associate Professor of civil engineering at the University of Toronto. He received his BASc from the University of Waterloo, Waterloo, ON, Canada, in 1994, and his PhD from the University of Toronto in 2000. He is Chair of ACI Committee 365, Service Life Prediction, and a member of Joint ACI-ASCE Committee 445, Shear and Torsion.*

Gian Michele Calvi *is Professor, Vice-Rector for Research, and Director of the Centre for Research and Graduate Studies in Understanding and Managing Extremes (UME) at IUSS. He received his MSc from the University of California, Berkeley, Berkeley, CA, and his PhD from the Politecnico di Milano, Milan, Italy. His research interests include displacement-based design and seismic isolation.*

ACI Honorary Member **Michael P. Collins** *is a University Professor of Civil Engineering at the University of Toronto. He is a member of Joint ACI-ASCE Committee 445, Shear and Torsion.*

REFERENCES

1. Priestley, M. J. N.; Calvi, G. M.; and Kowalsky, M. J., *Displacement-Based Seismic Design of Structures*, IUSS Press, Pavia, Italy, 2007, 721 pp.

2. Pampanin, S.; Kam, W.; Akguzel, U.; Tasligedik, A.; and Quintana-Gallo, P., "Seismic Performance of Reinforced Concrete Buildings in the Christchurch CBD in 22 February 2011 Earthquake—Part 2: Damage Observation," University of Canterbury Department of Civil and Natural Resources Engineering, Christchurch, New Zealand, 2012, 619 pp.

3. Priestley, M. N.; Verma, R.; and Xiao, Y., "Seismic Shear Strength of Reinforced Concrete Columns," *Journal of Structural Engineering*, ASCE, V. 120, No. 8, 1994, pp. 2310-2329. doi: 10.1061/(ASCE)0733-9445(1994)120:8(2310)

4. Stevens, N. J.; Uzumeri, S.; and Collins, M. P., "Reinforced Concrete Subjected to Reversed Cyclic Shear—Experiments and Constitutive Model," *ACI Structural Journal*, V. 88, No. 2, Mar.-Apr. 1991, pp. 135-146.

5. Okamura, H.; Maekawa, K.; and Izumo, J., "Reinforced Concrete Plate Element Subjected to Cyclic Loading," *IABSE Colloquium*, V. 54, Delft, the Netherlands, 1987, pp. 575-590.

6. Ohomori, N.; Tsubota, H.; Inoue, N.; Kurihara, K.; and Watanabe, S., "Reinforced Concrete Membrane Elements Subjected to Reversed Cyclic In-Plane Shear Stress," *Nuclear Engineering and Design*, V. 115, No. 1, 1989, pp. 61-72. doi: 10.1016/0029-5493(89)90260-4

7. Vecchio, F. J., "Towards Cyclic Modeling of Reinforced Concrete," *ACI Structural Journal*, V. 96, No. 2, Mar.-Apr. 1999, pp. 193-202.

8. Rose, B.; Shing, P. B.; Spacone, E.; and William, K., "Modeling of the Shear Behaviour of RC Members," 7th US National Conference on Earthquake Engineering, Boston, MA, 2002, pp. 166-169.

9. Mansour, M., and Hsu, T., "Behavior of Reinforced Concrete Elements Under Cyclic Shear: Part II—Theoretical Model," *Journal of Structural Engineering*, ASCE, V. 131, No. 1, 2005, pp. 54-65. doi: 10.1061/(ASCE)0733-9445(2005)131:1(54)

10. Palermo, D., and Vecchio, F. J., "Simulation of Cyclically Loaded Concrete Structures Based on the Finite Element Method," *Journal of Structural Engineering*, ASCE, V. 133, No. 5, 2007, pp. 728-738. doi: 10.1061/(ASCE)0733-9445(2007)133:5(728)

11. Gerin, M., and Adebar, P., "Accounting for Shear in Seismic Analysis of Concrete Structures," 13th World Conference on Earthquake Engineering, Vancouver, BC, Canada, 2004, 15 pp.

12. Uluğtekin, D., "Analytical Modeling of Reinforced Concrete Panel Elements under Reversed Cyclic Loadings," master's dissertation, Boğaziçi University, Istanbul, Turkey, 2010, 111 pp.

13. Ruggiero, D. M. V., "The Behaviour of Reinforced Concrete Subjected to Reversed Cyclic Loads," PhD dissertation, University of Toronto, Toronto, ON, Canada, 2015, 433 pp.

14. Saito, M.; Tanabe, I.; Furukawa, H.; Muramatsu, Y.; Ito, H.; Tsubota, H.; Watanabe, S.; and Kusama, K., "Experimental Investigations on Reinforced Concrete Panels for RCCV under In-Plane Shear Loading," *Summaries of Technical Papers of Annual Meeting Architectural Institute of Japan, Structures I*, 1985, pp. 817-818. (in Japanese)

15. Kurihara, K.; Ohmori, N.; Takahashi, T.; Tsubota, H.; and Watanabe, S., "Experimental Study on Nonlinear Behaviour of Reinforced Concrete Panels Subjected to In-Plane Combined Shear and Normal Stresses: Part 1, Outline and Results of CR Series," *Summaries of Technical Papers of Annual Meeting Architectural Institute of Japan, Structures II*, 1990, pp. 663-664. (in Japanese)

16. Watanabe, S.; Ohmori, N.; Takahashi, T.; Tsubota, H.; and Kurihara, K., "Experimental Study on Nonlinear Behaviour of Reinforced Concrete Panels Subjected to In-Plane Combined Shear and Normal Stresses, Part 3, Outline and Results of TR Series," *Summaries of Technical Papers of Annual Meeting Architectural Institute of Japan, Structures II*, 1991, pp. 431-432. (in Japanese)

17. Villani, R. D., "Reinforced Concrete Subjected to Cyclic Loads: A Pilot Study," BASc thesis, University of Toronto, Toronto, ON, Canada, 1995, 147 pp.

18. Vecchio, F. J., and Collins, M. P., "The Modified Compression Field Theory for Reinforced Concrete Elements Subjected to Shear," *ACI Journal Proceedings*, V. 83, No. 2, Mar.-Apr. 1986, pp. 219-231.

19. Kirschner, U., and Collins, M. P., "Investigating the Behaviour of Shear and Tension," Publication No. 87-02, Department of Civil Engineering, University of Toronto, Toronto, ON, Canada, 1987, p. 308

20. Khalifa, J., "Limit Analysis and Design of Reinforced Concrete Shells," PhD dissertation, University of Toronto, Toronto, ON, Canada, 1986, 312 pp.

21. Moehle, J., *Seismic Design of Reinforced Concrete Buildings*, McGraw-Hill Education, New York, 2014, 784 pp.

22. Bentz, E. C.; Vecchio, F. J.; and Collins, M. P., "The Simplified Modified Compression Field Theory for Calculating the Shear Strength of Reinforced Concrete Elements," *ACI Structural Journal*, V. 103, No. 4, July-Aug. 2006, pp. 614-624.

23. Mardia, K., *Statistics of Directional Data*, Academic Press Inc., London, UK, 1972, 357 pp.

24. Calvi, P. M., "A Theory for the Shear Behaviour of Cracks Providing a Basis for the Assessment of Cracked Reinforced Concrete Structures," PhD dissertation, University of Toronto, Toronto, ON, Canada, 2015, 346 pp.

25. Collins, M. P., and Mitchell, D., *Prestressed Concrete Structures*, Prentice-Hall, Englewood Cliffs, NJ, 1991, 766 pp.

26. Gylltoft, K., "A Fracture Mechanics Model for Fatigue in Concrete," *Matériaux et Construction*, V. 17, No. 1, 1984, pp. 55-58. doi: 10.1007/BF02474057

27. Zanuy, C.; de la Fuente, P.; and Albajar, L., "Estimation of Parameters Defining Negative Tension Stiffening," *Engineering Structures*, V. 32, No. 10, 2010, pp. 3355-3362. doi: 10.1016/j.engstruct.2010.07.009